Spin-Orbit Mediated Interference in the Radiative and Nonradiative Channels of the La 4d Core Resonances

E. Suljoti,[1,2,*] F. M. F. de Groot,[2] M. Nagasono,[1] P. Glatzel,[3] F. Hennies,[1] M. Deppe,[1] A. Pietzsch,[1] B. Sonntag,[1] A. Föhlisch,[1,†] and W. Wurth[1,‡]

[1]*Department of Physics, University of Hamburg, 22761 Hamburg, Germany*
[2]*Department of Chemistry, Utrecht University, 3584 CA Utrecht, The Netherlands*
[3]*European Synchrotron Radiation Facility (ESRF), 38043 Grenoble Cedex, France*
(Received 3 July 2009; published 25 September 2009)

Symmetrical fluorescence yield profiles and asymmetrical electron yield profiles of the preresonances at the La $N_{IV,V}$ x-ray absorption edge are experimentally observed in $LaPO_4$ nanoparticles. Theoretical studies show that they are caused by interference effects. The spin-orbit interaction and the giant resonance produce symmetry entangled intermediate states that activate coherent scattering and alter the spectral distribution of the oscillator strength. The scattering amplitudes of the electron and fluorescence decays are further modified by the spin-orbit coupling in the final $5p^5 \varepsilon l$ and $5p^5 4f^1$ states.

Electron correlation couples the motion of the electrons in many-electron atoms and causes the breakdown of the independent electron picture. The most prominent and well understood correlation effect is the configuration interaction mixing of discrete and continuum states which gives rise to autoionization [1–3]. Coherent population of continuum and resonance states leads to interference of both channels resulting in asymmetrical Fano profiles [1] in absorption spectra. Correlation can also cause configuration interaction among continuum states giving rise to photoionization interchannel coupling [4]. This effect can strongly influence the photoionization cross section not only near threshold [5] but also at intermediate and high photoelectron energies [6,7]. Spin-orbit interaction, an inherent aspect of electron correlation, can couple different photoionization channels and thereby produce new structures in the photoionization cross section [8] and generate significant changes in the photoelectron angular distribution [9]. In addition, spin-orbit coupling is reported to induce an inhomogeneous mixed-spin state in $LaCoO_3$ system and stimulate magnetic transitions [10]. The leverage of spin-orbit interaction to the magnetic properties and the charge, orbital, and spin ordering of the highly correlated materials is a subject of relevant research.

In this Letter, we investigate how the spin-orbit coupling in the intermediate and final states of resonant excitation and decay affects the interferences observed in the radiative and nonradiative decay channels of the $4d^9 4f^n$ preresonances at the $N_{IV,V}$ x-ray absorption edges of the lanthanides. Because of the localization of the $4f$ valence shell in these systems, the Coulomb and exchange interactions of the $4d$ core hole with the $4f$ electrons are very strong and result in tightly bound excited states and a significant multiplet splitting. Localization of the $4f$ shell gives rise to the large $4d - 4f$ dipole transition probability for the high energy components of the $4d^9 4f^n$ multiplet responsible for the giant resonance, approximately 10–

20 eV above threshold [11,12]. The $4d$-core hole spin-orbit interaction mixes the discrete preresonances and couples these states to the giant resonance. Furthermore, configuration interaction couples these states to the $4d^9 \varepsilon f$ continuum [1]. This is especially obvious for the giant resonance. The interaction with the continuum shifts its energy position downward [13] and causes its considerable width of approximately 10 eV [14]. At the positions of the preresonances, the tail of the giant resonance, even 20 eV below the maximum, displays a transition probability similar to that of the preresonances. As a consequence, the $4d$ excited states are highly correlated, best described by entangled quantum states. Photoexciting the lanthanides in the energy range of the preresonances results in coherent decay of these entangled states. The strong interference effects clearly manifest themselves in the asymmetrical profiles of the absorption lines.

In order to investigate electron correlation in lanthanides, we carried out x-ray absorption spectroscopy (XAS) and resonant inelastic x-ray scattering (RIXS) experiments at the $N_{IV,V}$ edges of light lanthanide ions (La, Ce, and Pr). In our studies, we focused on lanthanum, because within the lanthanide series it is ideally suited to disentangle the above mentioned phenomena. Lanthanum has no bound $4f$ electron in the ground state, and the multiplet effects give rise only to two $4d^9 4f^1$ $^3P_1$, $^3D_1$ preresonances located below the $4d^9 4f^1$ $^1P_1$ giant resonance. We report here highly resolved experimental spectra together with theoretical ones calculated for lanthanum ions. The influence of the molecular structure on the interference phenomena was found to be of a minor importance [15]. All of the experiments were performed on ligand capped $LaPO_4$ nanoparticles of 3–5 nm in diameter [16]. Thin films of few nanoparticle monolayers were prepared on HF-passivated Si(100) surfaces [16]. Thin film preparation avoided spectral blurring of the weak preresonances caused by Coulomb charging in these insulators. The ex-

periments were carried out at the UE52 beam line of the
BESSY II synchrotron facility, in Berlin (Germany). All of
the XAS and RIXS measurements have been performed in
ultrahigh vacuum, in the movable Hamburg inelastic x-ray
scattering station, which is equipped with a (Scienta
XES 350) x-ray spectrometer. Total electron yield (TEY)
spectra were measured by monitoring the sample current
and the total fluorescence yield (TFY) spectra by monitor-
ing zero order light in the x-ray spectrometer. The syn-
chrotron beam was incident at an angle of 7° to the surface
plane. The photons were linearly polarized with their
polarization vector perpendicular to the sample plane.
The x-ray emission spectrometer detected the radiative
RIXS signal 7° off the electric field vector of the incident
radiation. Theoretical spectra were calculated in intermedi-
ate coupling using Cowan's relativistic Hartree-Fock code
[17] and Kramers-Heisenberg formulation [18]. All atomic
parameters have been calculated in the Hartree-Fock limit
and were scaled to 80% to include the effects of configu-
ration interaction [17]. Line broadening of the states, due to
core-state lifetime and experimental resolution, was in-
cluded by the convolution with a Lorentzian ($^3P_1$, $^3D_1$,
$\Gamma = 0.14$ eV; $^1P_1$ $\Gamma = 9$ eV) and a Gaussian (FWHM =
0.07 eV) deduced from the experiment.

In panel (1) of Fig. 1, experimental TEY and TFY
spectra of the $4d^9 4f^1$ $^3P_1$ and $^3D_1$ preresonances are
shown. It is evident that the profiles of the preresonances
are asymmetric in TEY and nearly symmetric in TFY. In
addition, the peak maxima in TEY are shifted toward lower
energies. Theoretical atomic multiplet calculations showed
that spin forbidden transitions to the $^3P_1$ and $^3D_1$ states
become partially allowed due to mixing with the LS al-
lowed $^1P_1$ state, mediated via the $4d$ core hole spin-orbit
interaction. As a result, the three $^3P_1$, $^3D_1$, and $^1P_1$ states
are not pure $^{2S+1}L_J$ states but, in fact, are entangled states
that are linear combinations of the three pure $J = 1$ quan-
tum states. Both $^3P_1$ and $^3D_1$ states are ~96% pure, but the
$^1P_1$ symmetry contribution to the $^3D_1$ state (4.3%) is
3 times larger than that to the $^3P_1$ state (1.5%). Only
0.03% of the total oscillator strength of the $4d \rightarrow 4f$
transition is transferred to the $^3P_1$ state, and 0.29% is
transferred to the $^3D_1$ state, while transitions to the $^1P_1$
state comprise most of the oscillator strength, i.e., 99.67%.
Therefore, the intensity of the giant resonance is 100–
1000 times higher than that of the spin forbidden triplet
states. Approximating the giant resonance by a Lorentzian
results in the preresonances in a tail, the strength of which
is comparable to the strength of preresonances themselves.
By tuning the photon energy to the preresonances, the three
intermediate $^3P_1$, $^3D_1$, and $^1P_1$ states are coherently ex-
cited with comparable amplitudes giving rise to maximum
interference between the nonradiative scattering channels.
This explains the very asymmetrical electron yield profiles.
In the range of the preresonances the $4d^9 4f^1 \rightarrow$
$4d^{10} 5p^5 / 5s^1 \varepsilon l$ decays determine the total yield. The cal-
culated partial yield spectra, shown in panel (2) of Fig. 1,
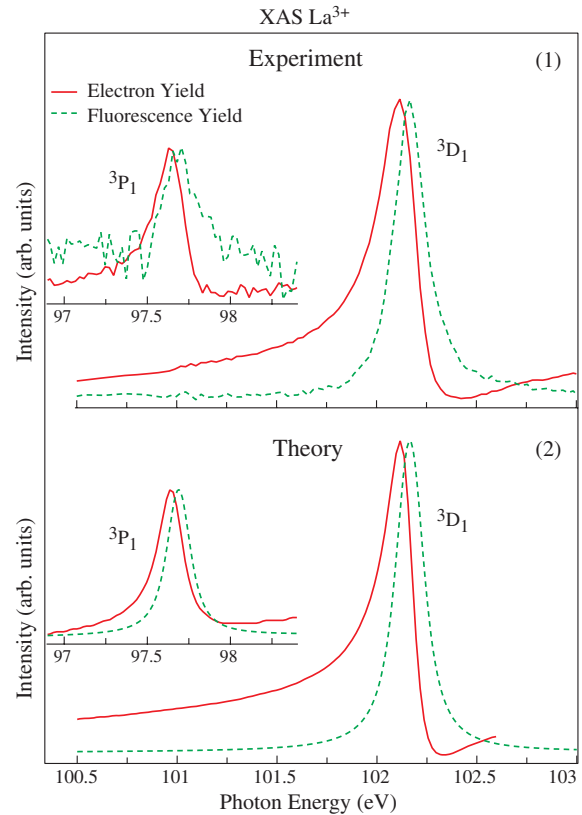

FIG. 1 (color online).   X-ray absorption spectra of the $^3P_1$ and
$^3D_1$ preresonances at the lanthanum $N_{IV,V}$ edge. Electron yield
and fluorescence yield show distinctly different line shapes.
(1) Experimental XAS spectra. (2) Calculated XAS spectra.
Experimental spectra are normalized to photon flux. All spectra
are normalized to unit peak height. The inset $^3P_1$ peak is
enlarged by a factor of 3.

closely resemble the measured ones. A schematic picture
of the excitation and nonradiative decay channels is given
in the left part of Fig. 2.

In contrast to the normal autoionization process which
gives rise to asymmetrical Fano profiles, our calculations
show that the interference of the direct photoionization
channels $5p/5s \rightarrow \varepsilon l$ with the core hole assisted channels,
discussed above, has a negligible effect on the line profiles.
The asymmetry of the line profiles is almost exclusively
due to the interference between the resonant channels. In
agreement with these results, Mishra *et al.* [19] have
reported that the interference of the direct and resonant
photoemission processes does not occur at the lanthanides
$4d$ preedges due to the absence of phase coherence. The
Coster-Kronig decay of the preresonances is much slower
than the fast direct photoemission process, leading to a
violation of the temporal match requirement for channel
interference.

But now we are confronted with the task of explaining
why the TFY spectra do not display any asymmetry. The
negligible influence of the direct $5p/s$ ionization channels
has eliminated the possibility to ascribe the asymmetry or
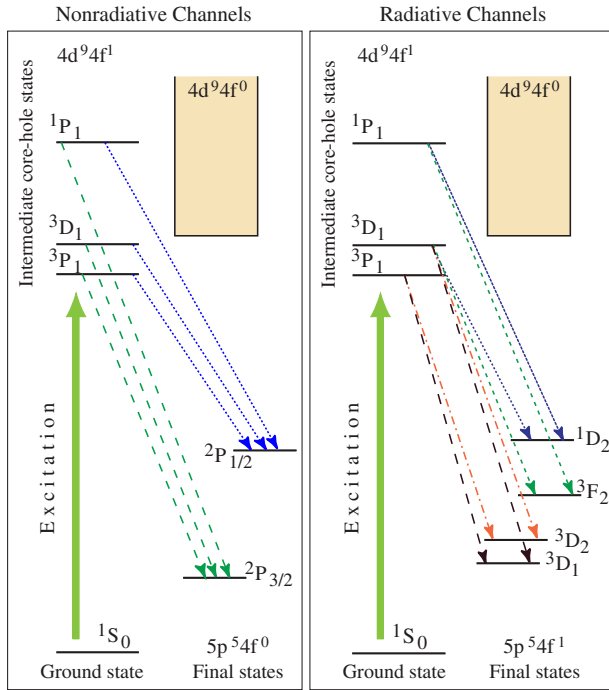symmetry in the TEY/TFY channel to the interference of

FIG. 2 (color online). Schematic of radiative and nonradiative decay channels of $N_{IV,V}$ resonances with a $5p$ hole in the final state. The scattering channels shown with the same color interfere due to the mixed intermediate states. Breaking of energy coherence in the final states of radiative decays, by the symmetry selection rule, decreases the number of interfering channels.

FIG. 3 (color online). Resonant inelastic x-ray scattering across the $^3D_1$ and $^3P_1$ resonances: (1) Experimental XAS spectra. The $^3P_1$ resonance is enlarged by a factor of 5. The shaded bars mark the excitation position and spectral bandwidth for the resonant inelastic x-ray scattering shown in panel (2). (3) Calculated RIXS spectra.

the resonant channel with the direct ionization channel for TEY and the missing of this interference in the TFY channel. To solve this puzzle we determined a series of fluorescence spectra by tuning the photon energy to selected energies in the range of the $^3D_1$ and $^3P_1$ preresonances. The fluorescence spectra covered the $4d4f$ elastic scattering (REXS) and the $4d5p$ inelastic scattering (RIXS); i.e., the energy transferred to the La ions (energy loss) ranged from 0 to 25 eV. The experimental $4d5p$ RIXS spectra are displayed in panel (2) of Fig. 3. Panel (1) gives the electron and fluorescence yield spectra of the $^3P_1$ and $^3D_1$ preresonances together with the photon energies at which the RIXS spectra have been taken. The fluorescence $^3D_1$, $^3D_2$, $^3F_2$, and $^1D_2$ lines are due to the radiative spectator decay $4d^94f^1 \rightarrow 5p^54f^1$. These radiative channels are schematically depicted on the right-hand side of Fig. 2. Note that our x-ray spectrometer could not resolve the $^3D_1$ and $^3D_2$ emission lines. By taking into account the spin-orbit mixing of the $4d^94f^1$ $^3P_1$, $^3D_1$, and $^1P_1$ resonances and the $5p^54f^1$ $^3D_1$, $^3D_2$, $^3F_2$, and $^1D_2$ final states, the RIXS spectra have been calculated within the Kramers-Heisenberg formalism. These calculations showed that the $^3P_1 \rightarrow {}^1D_2, {}^3F_2$ transitions comprise only 1.2% of the total strength of the $^3P_1$ resonance and the $^1P_1 \rightarrow {}^3D_1, {}^3D_2$ transitions comprise less than 0.5% of the strength of the $^1P_1$ resonance. For this reason these transitions are not included in Fig. 2. Consequently, not all possible transi-
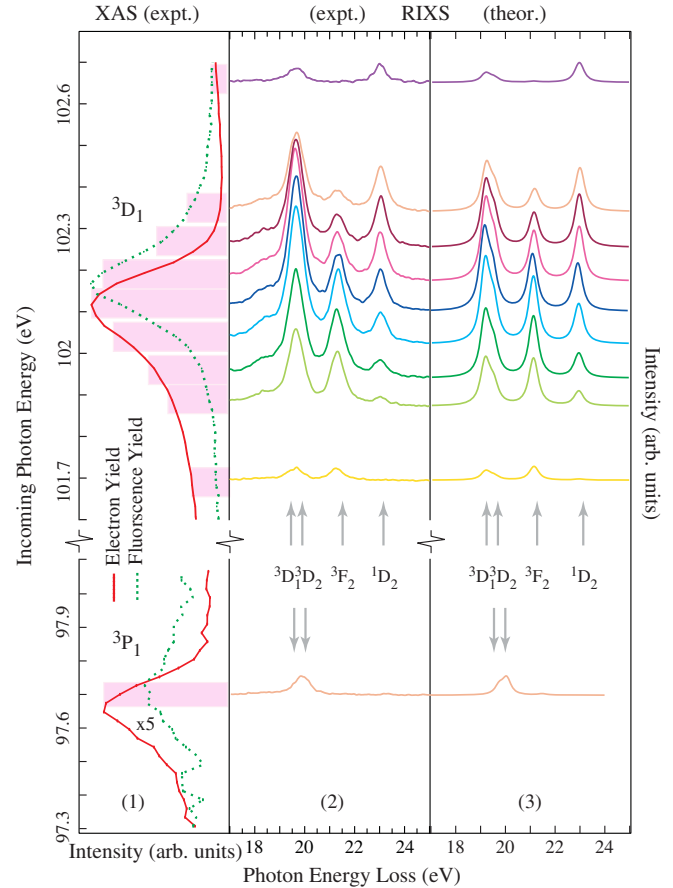
tions between the intermediate states and the final states contribute to the interference of the coherent radiative decay channels. This is different from the nonradiative decay, where every final state is reached from every intermediate state, as depicted in Fig. 2.

The experimental RIXS spectra reveal a normal resonant behavior for the unresolved $^3D_1, {}^3D_2$ emission line; its intensity closely follows the symmetric intensity profile of the $^3D_1$ resonance, whereas the $^3F_2$ $(^1D_2)$ emission line shows a highly asymmetric intensity profile (see Fig. 3), which reaches its maximum intensity at the low energy (high energy) flank of the $^3D_1$ resonance. This is clear evidence for the interference between the decay channels, which however is not visible in the absorption spectra (TFY). To understand this observation, RIXS calculations, in which the radiative decay is treated as a coherent excitation-deexcitation process, were performed. Theoretical spectra given in panel (3) of Fig. 3 reproduce the experimental spectra in panel (2) very well. Already the spectra in Fig. 3 indicate that adding up the intensities of the different fluorescence lines for each excitation energy
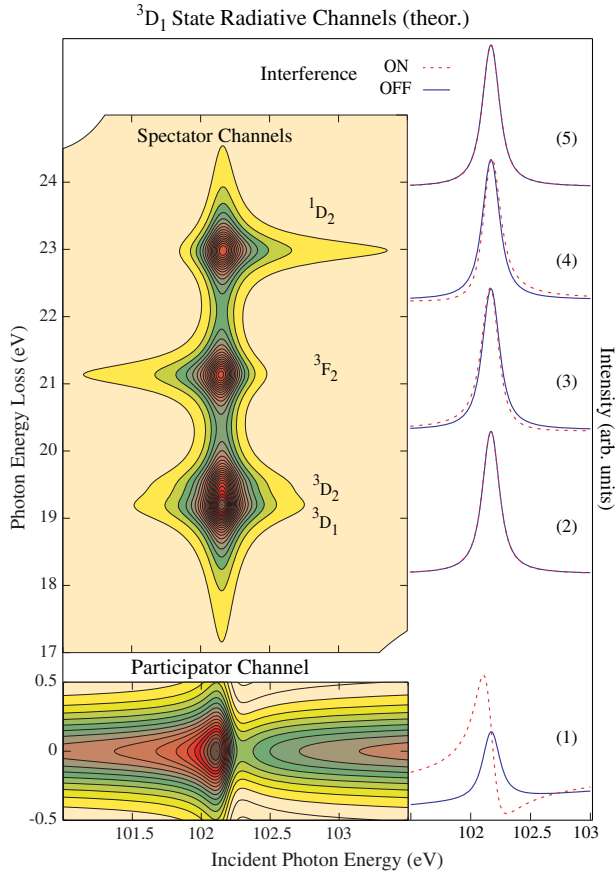
FIG. 4 (color online).   Theoretical model of resonant inelastic (upper panel) and elastic (lower panel) x-ray scattering across the $^3D_1$ La N-edge resonance, taking symmetry entanglement and channel interference into account. Right panel: Partial fluorescence yield (1–4) resulting from integrating the RIXS energy scale (hatched line). (5) is the sum of (3)–(4). Neglecting channel interference leads to Lorentzian line profiles (full line).

will result in a highly symmetrical curve very similar to the TFY of the $^3D_1$ preresonance determined experimentally. In order to substantiate this idea we calculated the partial fluorescence yield for all of the radiative spectator channels for excitations in the range of the $^3D_1$ resonance. The results are presented in Fig. 4. The $^1D_2$ and $^3F_2$ lines display a very distorted and asymmetric profile. Constructive interference causes an enhancement of the intensity of the $^1D_2$ ($^3F_2$) line at high (low) excitation energies. The unresolved ($^3D_2$, $^3D_1$) line shows an almost symmetric pattern. Integrating over the area of the fluorescence lines results in the line profiles given by the dashed lines (2), (3), and (4) in the right part of Fig. 4. Adding the line profiles (3) and (4) results in the symmetric profile (5). The asymmetries of lines (3) and (4) almost exactly cancel each other. This explains why, in spite of the strong interference effects, the profile of the $^3D_1$ TFY is symmetric. It is interesting to note that neglecting interference effects results in almost identical profile (5), whereas profiles (3) and (4) show marked differences. Finally, we discuss the

elastic $4d^9 4f^1 \rightarrow 4d^{10}$ participator channel, which might also contribute to TFY. The calculated participator channel exhibits an asymmetric profile as shown in the bottom panel and line (1) of Fig. 4. But since the probability of this decay channel is 100 times smaller than that of the spectator decays, its contribution to the TFY is negligible.

In conclusion, we have experimentally detected asymmetric TEY and symmetric TFY line profiles of the La N-edge preresonances. Theoretical calculations revealed that the localized preresonances and the giant resonance are mixed due to the $4d$ spin-orbit interaction. This gives rise to interference between the different excitation and decay channels clearly manifesting itself in the asymmetric TEY profiles. In the case of the spectator channels, the radiative decay leads to final states strongly mixed by the $5p$ spin-orbit interaction. This results in two channels of almost equal strength and opposite scattering amplitudes displaying lines of opposite asymmetry. By adding up all of these contributions, the asymmetries cancel, giving rise to a symmetric TFY profile. Spin-orbit mixing of the intermediate and the final states is the essential mechanism responsible for the startling results.

*e.suljoti@uu.nl
†alexander.foehlisch@desy.de
‡wilfried.wurth@desy.de

[1] U. Fano, Phys. Rev. **124**, 1866 (1961).
[2] U. Fano and J. Cooper, Phys. Rev. **137**, A1364 (1965).
[3] F. H. Mies, Phys. Rev. **175**, 164 (1968).
[4] U. Fano and J. Cooper, Rev. Mod. Phys. **40**, 441 (1968).
[5] V. Schmidt, Rep. Prog. Phys. **55**, 1483 (1992).
[6] E. Dias et al., Phys. Rev. Lett. **78**, 4553 (1997).
[7] M. Amusia et al., Phys. Rev. Lett. **85**, 4703 (2000).
[8] M. Amusia et al., Phys. Rev. Lett. **88**, 093002 (2002).
[9] M. Amusia et al., J. Phys. B **37**, 937 (2004).
[10] M. Haverkort et al., Phys. Rev. Lett. **97**, 176405 (2006).
[11] J. L. Dehmer et al., Phys. Rev. Lett. **26**, 1521 (1971).
[12] A. F. Starace, Phys. Rev. B **5**, 1773 (1972).
[13] U. Köble et al., Phys. Rev. Lett. **74**, 2188 (1995).
[14] M. Richter et al., Phys. Rev. A **39**, 5666 (1989).
[15] E. Suljoti, Ph.D. thesis, Hamburg University, 2008.
[16] E. Suljoti et al., J. Chem. Phys. **128**, 134706 (2008).
[17] R. D. Cowan, The Theory of Atomic Structure and Spectra (University of California Press, Berkeley, 1981).
[18] F. de Groot and A. Kotani, Core Level Spectroscopy of Solids (Taylor & Francis, London, 2008).
[19] S. R. Mishra et al., Phys. Rev. Lett. **81**, 1306 (1998).